Exploiting Piecewise Linearity in Wave Energy Converters

A Thesis

Presented in Partial Fulfillment of the Requirements for the Degree Master of Science in the Graduate School of The Ohio State University

By

Paul Gusmano, B.S.

Graduate Program in Mechanical Engineering

The Ohio State University

2025

Master's Examination Committee:

Kiran D'Souza, Advisor

Hanna Cho

Abstract

Researchers have developed many novel ways to scavenge energy from otherwise unused sources. One of the most abundant sources of predictable energy can be found in ocean waves. Wave Energy Converters (WECs) are a class of energy harvester that operate at the surface of the ocean, excited by waves. This work shows how introducing a controllable mechanical stopper to a WEC can improve its performance. The performance of the adjustable stopper is tested in Wave Energy Converter Simulator (WEC-Sim), open-source software for simulating WECs. The WEC with the stopper is compared against the same reference model without the stopper to demonstrate its effectiveness, getting upwards of a 25% increase in power output. A simple controller is developed using steady-state sea responses. This controller helps improve the power output of WECs by actively shifting their resonant frequencies to adjust WEC responses. The design shows improved performance in steady-state sea conditions. The controller is also tested in noisy and quasi-static sea states to compare the novel WEC against the baseline uncontrolled WEC.

Dedicated to my God and my Neighbors

Acknowledgments

I'd like to express my deepest gratitude to everyone who has supported me on my academic journey. My graduate advisor, Dr. Kiran D'Souza, has been an essential guide, providing direction both academically and professionally during my time in the Nonlinear Dynamics and Vibrations Lab. Yuqin Guan, a PhD. student in the lab, has been a consistent source of encouragement and expertise during my time here. The faculty of Cedarville University, especially Dr. Luke Fredette, helped me cultivate a deep curiosity for the natural and abstract world through their instruction and support, and I would not have pursued a graduate degree if not for their effort.

I'd like to thank family and friends who have shaped me into who I am. Their love, encouragement, and support have helped me persevere, especially through graduate school. Of those people, I'd like to mention my parents, who have modeled the importance of hard work and a love for community. I also want to give thanks to my fiancée, Maddie. She's become my closest friend, and her love shapes me to be a better man.

Finally, I want to give thanks to the Triune God, whose death, burial, and resurrection in the person of Jesus Christ provides forgiveness for sins and proves my worth. His sacrifice motivates hard work, and leaves room for rest. Even if everything else is lost, I know that He loves me, and that is enough.

Vita

May 2023	B.S. Mechanical Engineering Cedarville University, USA
August 2023–August 2024	Presidential Fellow The Ohio State University, USA
August 2024–Present	Graduate Teaching Assistant Department of Mechanical and Aerospace Engineering The Ohio State University, USA
August 2023–Present	M.S. Mechanical Engineering The Ohio State University, USA

Publications

Research Publications

P. Gusmano, L. Fredette "Experimental Validation of Vibration Isolation in Quasi-Zero Stiffness Mount Concept". *SAE Technical Paper*, 2023-01-1066, May 2023.

Fields of Study

Major Field: Mechanical Engineering

Table of Contents

Page

List of Tables

Table **Page**

List of Figures

Chapter 1: Introduction

Energy harvesting is the practice of scavenging energy in mechanical, thermal, and other physical processes and converting it into useful electrical energy [13, 9]. Energy harvesting from the ocean has received more attention in recent decades [2, 10, 11, 20]. These energy harvesters, also known as marine energy converters (MECs), collect kinetic and potential energy from the surrounding marine environment. A special case of MEC are those designed to interact with waves, called wave energy converters (WECs). Researchers have developed various types of WECs such as oscillating water column, oscillating surge converter and overtopping converters. Among all types of WECs, oscillating body devices, also known as point absorbers [16], have the most potential due to their prospective use in deep offshore and array deployment. Point absorbers are floating, buoy-like devices that convert their up and down motion with ocean waves to power through a power take-off (PTO) system [15]. These systems are not considered mature compared to other renewable energy sources such as wind and solar. One main challenge for point absorber WECs is the variable nature of ocean waves [3]. Harsh ocean conditions significantly decrease their efficiency. To improve their efficiency and adaptability, researchers have developed reliable modeling tools and are looking for more advanced methodologies to enhance the performance of point absorber WECs.

While WECs have promising potential for energy harvesting, they are expensive to develop, and even evaluating a scale model requires a wave pool to conduct tests. Wave Energy Converter Simulator (WEC-Sim) is an open source tool developed to computationally simulate WECs as an intermediate step in the WEC development process [1, 21]. WEC-Sim has shown that it can accurately model sea states governed by linear wave theory [8, 18, 14]. WEC-Sim is built in MATLAB/Simulink and is a highly modular program, which enables users to test existing WEC models and custom WEC models with different designs.

One of the earliest and most common WECs is the linear WEC. Linear WECs typically have similar properties to linear mechanical models. The power generation and the vibration of the linear WECs are closely related. The WEC is at maximum vibration excited by a wave with the same frequency as its resonant frequency. When the frequency of the wave moves away from the resonant frequency of the WEC, the vibration of the WEC will decrease significantly. The actual input wave has a wide operational frequency due to the change of weather and wind conditions and thus will limit the overall power generation of the point absorber WEC under real ocean wave conditions. Multiple approaches have been tried to attempt to solve this challenge. However, most of the methods are either changing the geometry design of the system [22, 5] or improving the transfer method [7]. Little has been researched on improving the inherent dynamics of the WEC under changing excitations.

Recently, new designs that incorporate piecewise linear (PWL) systems into the energy harvester have been proposed [17]. It was shown that the PWL systems can significantly increase the operational frequency range while maintaining large vibration amplitudes. This new PWL energy harvester with a controllable gap size has also been demonstrated experimentally with an electromagnetic [19] and piezoelectric [6] energy generation implementation.

In this thesis, the introduction of a piecewise linearity into a WEC is investigated computationally. The PWL system is based on the Reference Model 3 (RM3), a preset two-point absorber model in the WEC-Sim library, with an adjustable stopper incorporated. A computational model of the PWL system is generated and tested to compare its performance with the standard linear model of the RM3. Then, a simple algorithm is discussed that can control the position of the stopper along the length of the RM3's spar component, with the goal of maximizing the average PTO power output in off-resonant sea states. After this, the controller is tested in different types of sea states to verify its robustness: regular sea states, noisy sea states, and quasi-static sea states. Finally, conclusions are presented and grounds for future work are discussed.

Chapter 2: Developing a Controllable-Gap Stopper

2.1 Introduction

This chapter first describes how a controllable-gap stopper was implemented in WEC-Sim, then describes how a simple lookup-table-based controller was developed to control its position and improve power output.

2.2 Stopper Implementation in WEC-Sim

The system dynamics of a wave energy converter (WEC) can be represented by solving the Cummins equation [4]. The equation of motion (EOM) of the WEC, simplified to remove terms irrelevant to the following investigation, is given in Equation (2.1).

$$M\ddot{\mathbf{x}} = \mathbf{F}_{exc} + \mathbf{F}_{rad} + \mathbf{F}_{PTO} + \mathbf{F}_{B}, \tag{2.1}$$

where M is the mass matrix, $\mathbf{x}$ is the translational and angular positions of every degree of freedom in the simulation, $\mathbf{F}_{exc}$ is the wave excitation force and torque vector, $\mathbf{F}_{rad}$ is the force and torque vector due to wave radiation, $\mathbf{F}_{PTO}$ is the PTO force and torque vector, and $\mathbf{F}_{B}$ is the net buoyancy restoring force and torque vector [21]. Note that all the mentioned forces, except for $\mathbf{F}_{PTO}$, are hydrodynamic and result from a body's interaction with waves.

The WEC studied in this thesis, Sandia's RM3, is shown in Figure 2.1 for reference (not drawn to scale). As a two-body, floating point absorber, it is composed of two main bodies: the float, designed to float on the water's surface, and the spar, a body designed to remain stable, so the float can move relative to it.

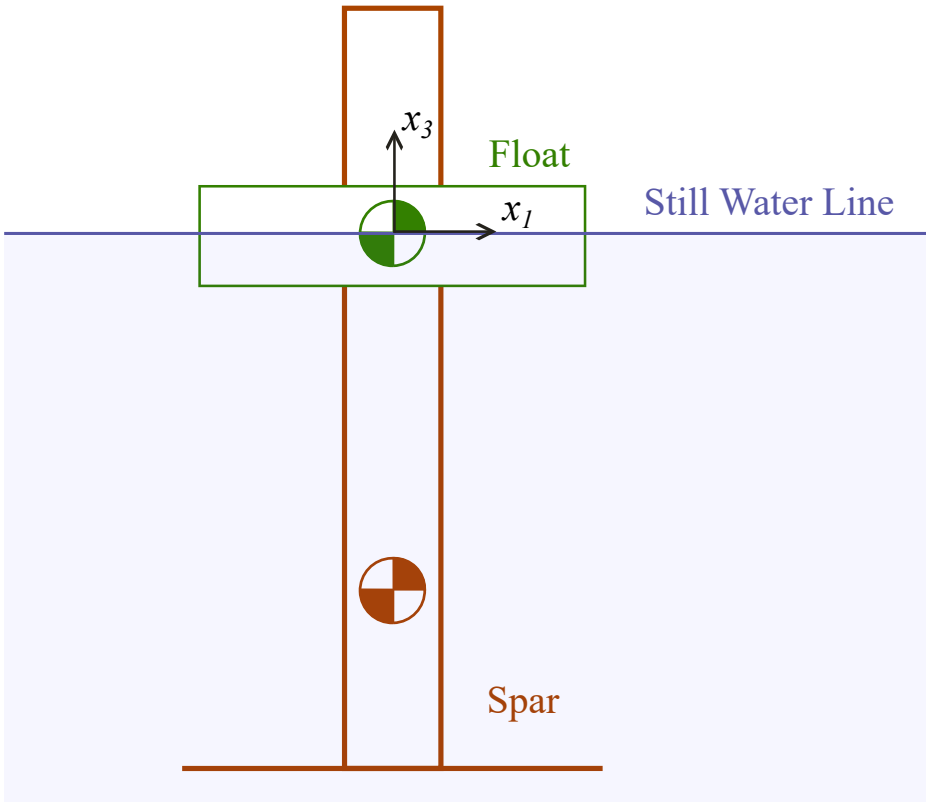

Figure 2.1: Sandia's Reference Model 3 (RM3)

To implement a stopper to the RM3, the RM3 model provided with WEC-Sim was modified to access the position and velocity of the two bodies for each point in time. WEC-Sim calculates the surge, heave, sway, pitch, roll and yaw for each body in the simulation

at every point in time, so that every rigid body contributes six degrees of freedom to the simulation. These values are calculated in Simulink at each point in time by numerically solving Equation (2.1). With simple modifications to the "body" blocks provided in WEC-Sim, the positions and velocities of each of these bodies can be obtained. After getting the positions and velocities of each body, simple trigonometry can be used to find the relative position $\mathbf{x}_r$ between the two bodies' centroids. This is detailed below in Figure 2.2 using, without loss of generality, a two-dimensional example. First, a unit vector $\mathbf{u}_a$ is developed

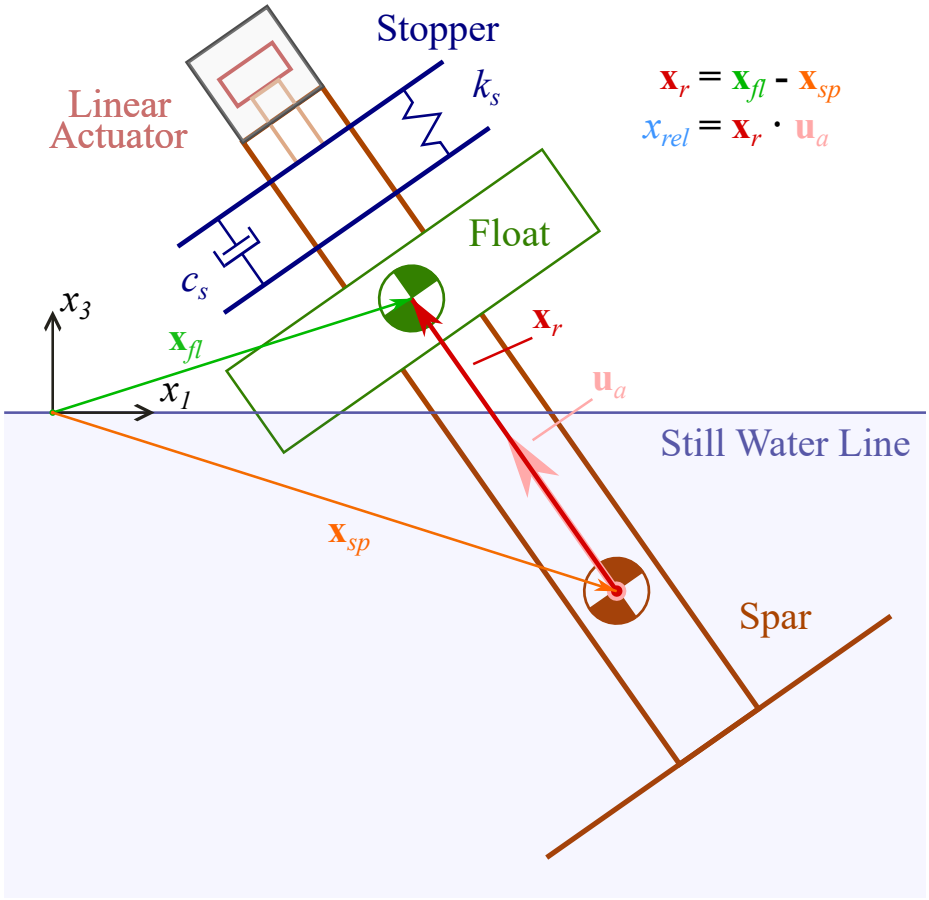

Figure 2.2: Stopper-Included RM3 System, detailing how to calculate x_{rel}

between the centroids representing each body by finding the relative position vector between them at the first point in time $\mathbf{x}_{r0}$ and dividing it by its magnitude. Assuming the relative motion of these centroids occurs along a central axis, as is the case with the RM3, the orientation of this unit vector through time can be given by the pitch, roll, and yaw of the base body. At each point in time, Simulink returns the position of each bodies' centroid ($\mathbf{x}_{fl}$ and $\mathbf{x}_{sp}$ in the RM3's case.) Next, the difference in positions of the these centroids $\mathbf{x}_r = \mathbf{x}_{fl} - \mathbf{x_{sp}}$ are taken to get the relative position between the two bodies. Then, the dot product of $\mathbf{u}_a$ and $\mathbf{x}_r$ are taken to get a scalar representation x_{rel} of $\mathbf{x}_r$. Because $\mathbf{u}_a$ and $\mathbf{x}_r$ are collinear by assumption, x_{rel} will always be the signed magnitude of $\mathbf{x}_r$. The same steps detailed above can be used to find the relative velocity between the two bodies $\dot{x}_{rel}$ if the velocity vectors calculated by WEC-Sim are considered instead of the position vectors.

The analysis of axisymmetric WECs like the RM3 can be simplified by considering $\mathbf{u}_a$ as the basis vector for a new, one-dimensional coordinate along its central axis. Assuming all the relative motion between the two WEC bodies can be expressed in terms of this coordinate, that the bodies maintain the same orientation relative to one another, and that the WEC responds primarily in heave, the system can be thought of as a one degree of freedom mass-spring-damper system subject to base excitation and a hydrodynamic forcing function.

If the RM3 is put in these terms, its float, moving relative to its spar, serves as the mass while its PTO, idealized in terms of a stiffness and damping, serves as the spring and damper. The relative displacement between the two bodies' centroids $\Delta x_{rel} = x_{rel} - x_{rel0}$ behaves as the coordinate. Furthermore, if a stopper is designed so that it deflects along $\mathbf{u}_a$, it can easily be included as a contacting mass so that the float experiences intermittent contact. If the stopper is positioned so that a gap $g_s(t)$ exists between it and the float's initial

position, a simple model describing the force it exerts on the float is given by

$$F_s = \left(k_s \left(\Delta x_{rel} - g_s\right) + c_s \left(\Delta \dot{x}_{rel} - \dot{g}_s\right)\right) u_s \left(\Delta x_{rel} - g_s\right), \tag{2.2}$$

where F_s is the reaction force of the stopper applied to the PTO, $u_s(x)$ is the unit step function, and k_s and c_s are the stiffness and damping of the stopper, respectively. This abstraction of the RM3 with the stopper included, along with the kinematics discussed above, is shown in Figure 2.3.

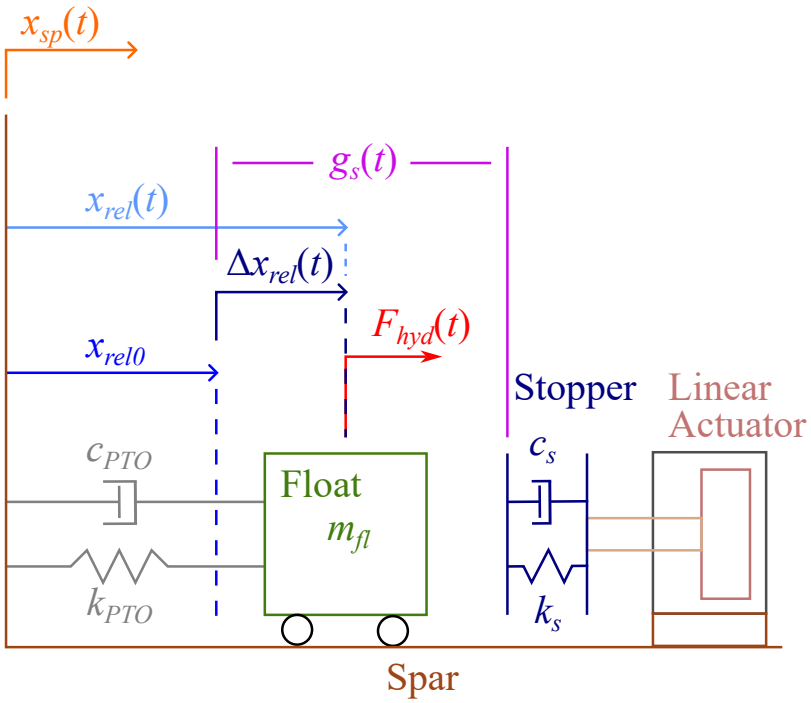

Figure 2.3: RM3 Abstracted Into a Stopped Mass Spring Damper System, Including Kinematics

To understand $g_s(t)$, consider Figure 2.4. Figure 2.4a shows that $g_s > 0$ corresponds to when there's a gap between the stopper's current position and the float's initial position.

$g_s = 0$ means that the stopper is flush against the float's initial position. Figure 2.4b explains that, if $g_s < 0$ the stopper's position penetrates into the float's initial position. If $k_s \neq 0$, this corresponds to a prestress in the stopper. Whenever $\Delta x_{rel} > g_s$, the RM3 is said to be in a closed state. If $\Delta x_{rel} > g_s$ for all time, the RM3 is said to be fully closed. Similarly, when $\Delta x_{rel} \leq g_s$, the RM3 is said to be in an open state. If this condition holds for all time, the RM3 is said to be in a fully open state.

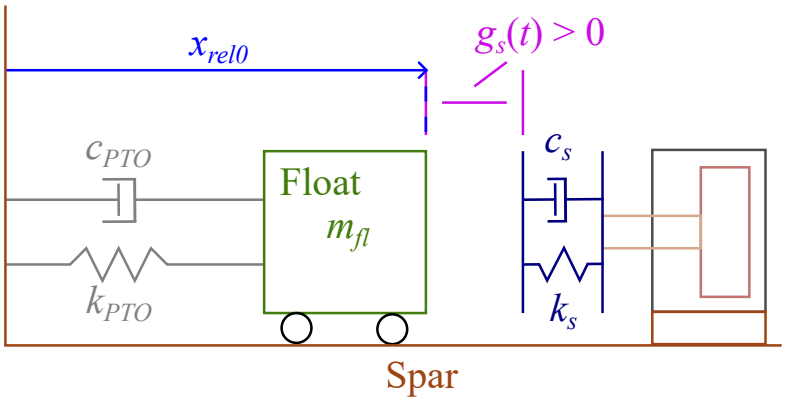

(a) $g_s > 0$

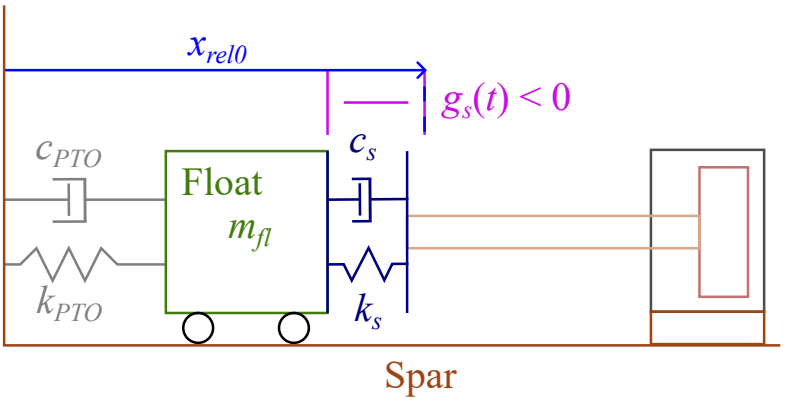

(b) $g_s \leq 0$

Figure 2.4: $g_s(t)$ Explained

By defining $\mathbf{u}_a$, projecting all the coordinates and forces onto it, and by adding F_s, Equation (2.1), which describes the evolution of the translational and angular positions of each body in time, can be simplified to a scalar-valued equation describing the displacement of the float relative to the spar, given by

$$m_{fl}\Delta\ddot{x}_{rel} + c_{PTO}\Delta\dot{x}_{rel} + k_{PTO}\Delta x_{rel} = c_{PTO}\dot{x}_{sp} + k_{PTO}x_{sp} + F_s(t) + F_{hyd}(t), \tag{2.3}$$

where F_{hyd} is the sum of all the hydrodynamic forces mentioned in Equation (2.1) projected onto $\mathbf{u}_a$, $x_{sp} = \mathbf{x}_{sp} \cdot \mathbf{u}_a$ and assuming k_{PTO} is unstretched when $\Delta x_{rel} = 0$.

To practically implement this in WEC-Sim, Δx_{rel} and $\Delta\dot{x}_{rel}$ were obtained using the process described above. Next, Δx_{rel} and $\Delta\dot{x}_{rel}$ were used to calculate F_s using Equation (2.2) and an arbitrary selection of $g_s(t)$. Then F_s was negated to serve as a reaction force, and passed into a "Translational PTO Actuation Force" block (provided in WEC-Sim) to simulate contact between the float and stopper.

2.3 Controller Design

To develop a controller to control $g_s(t)$, an arbitrary $c_s = 5$ MNs/m and $k_s = 0$ were selected. Then, power matrices with energy period $T_e = \{2,\ 3,\ \ldots, 18\}$ s, and significant wave height $H_s = \{0.5.\ 0.75,\ \ldots,\ 2\}$ m were developed for the stopper-controlled RM3 at 10 values of g_s ranging between -60 and 95 cm. To develop the power matrices, each sea state and g_s combination was simulated for 400 seconds. WEC-Sim applied a ramp function to the wave for a specified ramp time of 100 seconds, so data prior to this time was neglected. WEC-Sim calculates the instantaneous mechanical power at each point in time, so the last 300 seconds of instantaneous power data were used to calculate the average power output of the PTO $\bar{P}_{out}$. After power matrices were developed for each value of g_s, they were compared against one another to see which value of g_s produced the highest $\bar{P}_{out}$ for a

given sea state. A simple, rule-based controller was developed based on the comparison of those power matrices. For more information on how this was done programmatically, see Appendix A.

Figure 2.5 shows the resulting lookup table that was developed to select g_s for different sea states. Figure 2.6 shows the resulting percent increase in $\bar{P}_{out}$. Though this stopper was tested in a wider range of sea states, it only saw improvements in $\bar{P}_{out}$ for $T_e \in [8,\ 18]$ s. This happens because the RM3 was designed for a particular wave site in Eureka, California [12]. Consequently, the RM3 was designed to resonate at the energy periods most represented in the joint probability distribution (JPD) of sea states at the site. The piecewise linearity (PWL) introduced by the stopper is naturally going to change the resonant frequency of the system. This means that it is better for the float and stopper to stay out of contact in these sea states. This principle is shown in Figure 2.7. The spike in power generation between $T_e = 15$ and 17 s, for example results from the excitation of a resonant frequency. If the stopper contacted the float in this region of sea states, the resonant frequency would change and the power generation would decrease significantly.

In operation, the controller receives estimations of the current sea state and energy period. These measurements are passed through a low-pass filter with a cutoff frequency of 0.2 Hz to handle sensor noise. The selection of 0.2 Hz is motivated by the Joint Probability Distribution (JPD) of the wave site included in the documents detailing the RM3 design [12], as the majority of sea states will have $T_e > 5$ s.

The steps of the control process are summarized below. They are also summarized schematically in Figure 2.8.

1. Pre-compute the stopper gap map for a given wave amplitude range and wave time period range that is expected to excite the buoy deployed at a particular location.

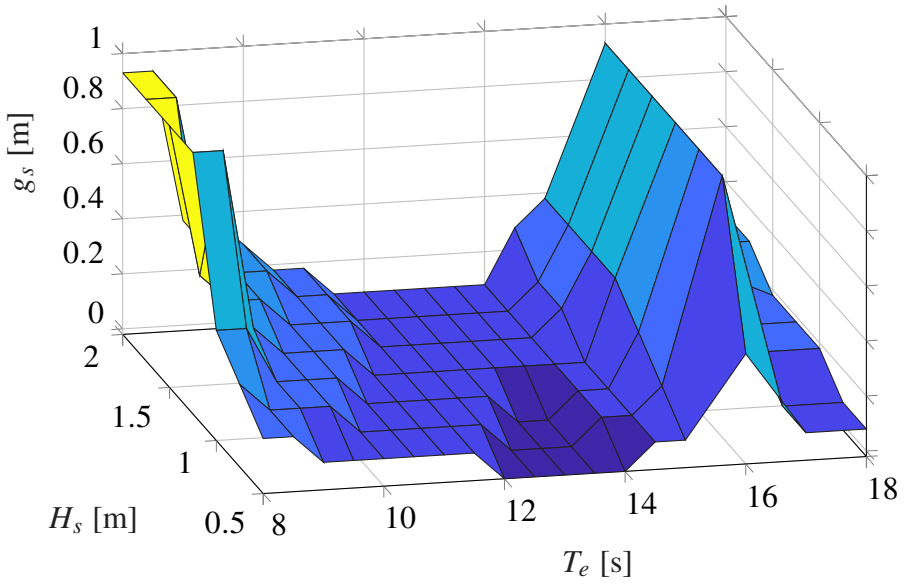

Figure 2.5: Optimal Stopper Gaps for Max Average Power Output $G(H_s, T_e)$ for $c_s = 5$ MNs/m, $k_s = 0$ N/m.

2. Measure the wave amplitude H_s and wave frequency T_e during operation.

3. Use H_s and T_e with the stopper gap map to compute the optimal gap value.

4. Use the computed optimal gap value to adjust the actual gap of the stopper during operation.

5. Repeat steps 2-4 during operation.

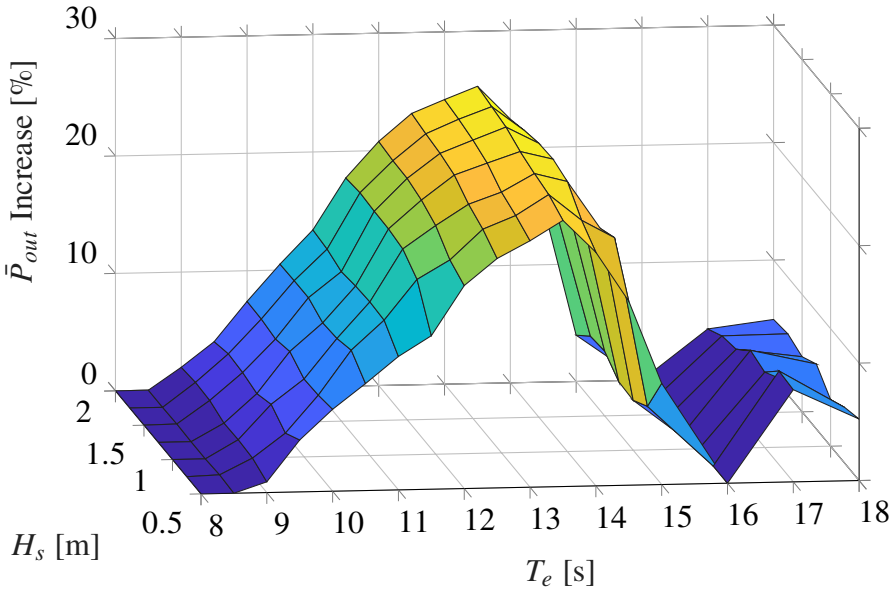

Figure 2.6: Percent Increase in Average PTO Power Output with a Properly-Positioned Stopper, $c_s = 5$ MNs/m, $k_s = 0$ N/m.

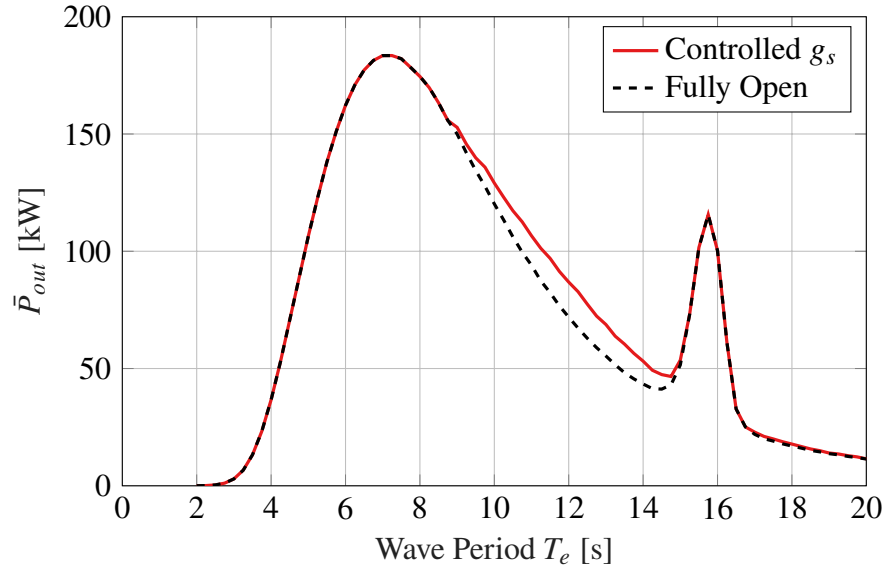

Figure 2.7: Power Generation in the Fully Open and Stopper-Controlled RM3, $H_s = 2$ m, $c_s = 5$ MNs/m, $k_s = 0$ N/m

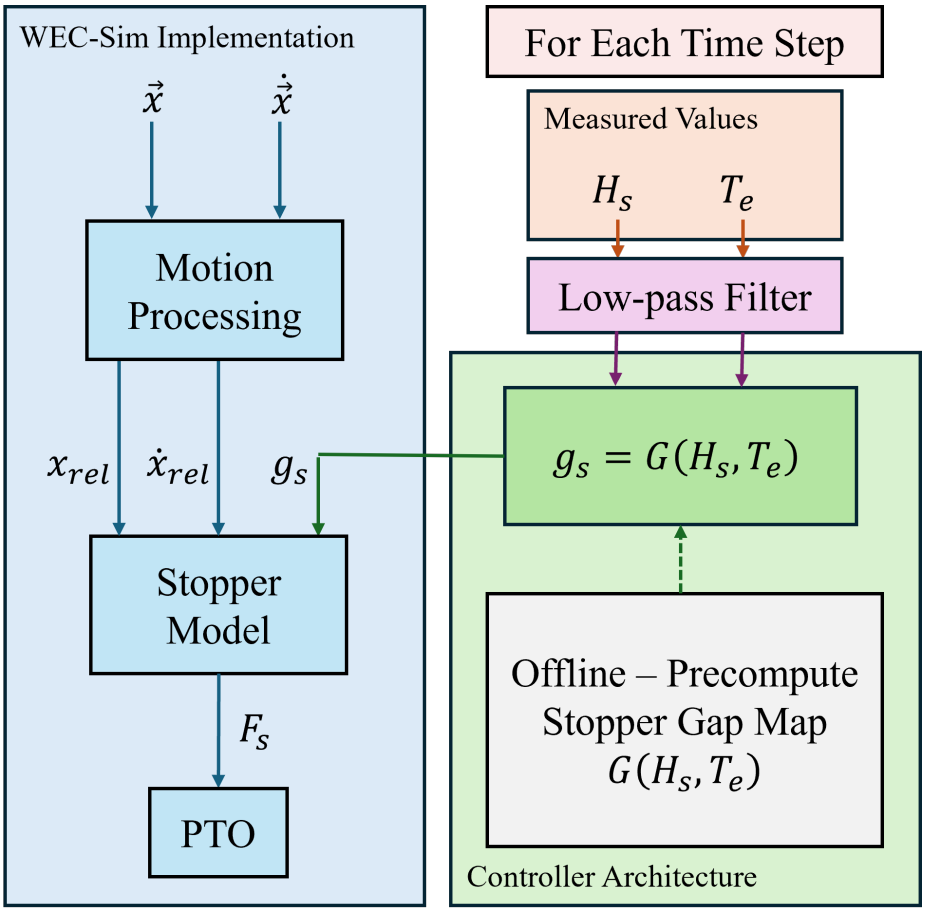

Figure 2.8: High-Level View of Implementation

Chapter 3: Stopper Effects in Various Wave Conditions

3.1 Regular Waves

To see the effects of the stopper on the RM3 in regular waves, it was tested in identical conditions, where $H_s = 2$ m and $T_e = 13.5$ s, with the only difference being the stopper gap g_s. The results of this are shown in Figures 3.1 to 3.3. Figure 3.1 shows how the float-stopper interaction effects Δx_{rel} in a given period. As the float moves along $\mathbf{u}_a$, it will engage the stopper when Δx_{rel} exceeds the gap size g_s. The float will then disengage from the stopper when Δx_{rel} is less than g_s. Note the difference in response when Δx_{rel} is greater than and less than g_s. Both responses are approximately sinusoidal, but the amplitude of the wave is less when $\Delta x_{rel} > g_s$. This is because the stopper imparts a large force to float as they're in contact. While this contact decreases the overall relative motion of the spar, it also increases the instantaneous power output P_{out}, as shown in Figure 3.2. This relationship between P_{out} and contact events is further discussed in Section 3.2.

To verify whether the controller correctly chooses the optimal gap, Figure 3.3 was developed to see if the controlled-stopper RM3 model developed the most energy compared to other choices of g_s. The choice of g_s is important because it can significantly affect the average power output of the RM3. In the fully open state, the RM3 produces an average power of 48.2 kW. At the optimal gap for this sea state, $g_s = 8$ cm, the average power

output is 58.9 kW, for an increase of 24.26%. If the stopper gap is too great for a given sea state, the improvement in power generation is diminished because the model cannot take full advantage of the stopper. If, for example, $g_s = 30$ cm, the average power output is 56.7 kW for an average power increase of only 17.70%. Or, if the stopper gap is too low for a given sea state, the average power output can actually *decrease* relative to the original RM3 model's power output for the same sea state. Choosing $g_s = -40$ cm produces an average power of 41.6 kW for a decrease in power of 13.70%. For the damping only stopper, the fully closed state produces the minimum power. In this case, the fully closed state produces 37.0 kW of power on average for a decrease in power of 23.2%.

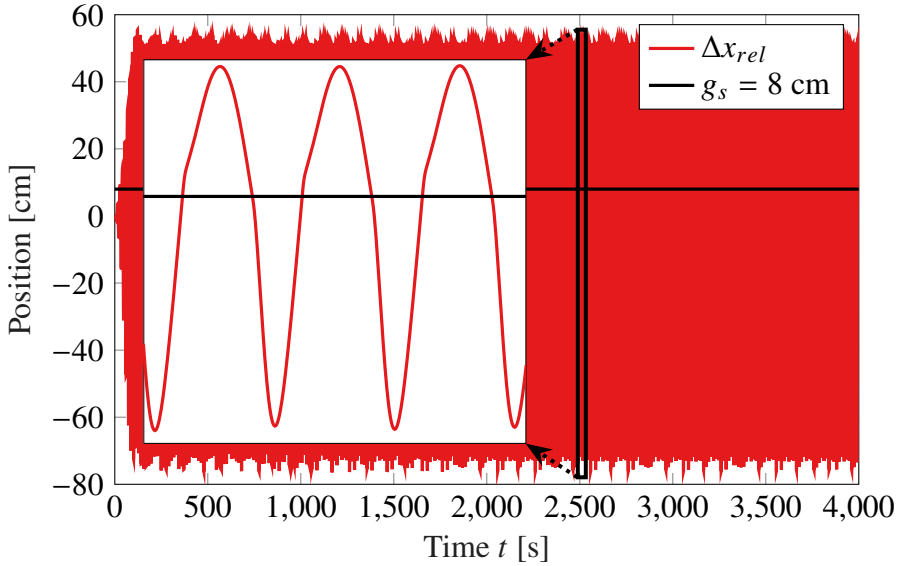

Figure 3.1: Engagement and Disengagement of the Float and Stopper, $H_s = 2$ m, $T_e = 13.5$ s

Figure 3.4 explains this relationship by plotting $\bar{P}_{out}$ as a function of g_s. The fully open (FO) region has a consistent $\bar{P}_{out}$ because the float and stopper never engage. Similarly, the

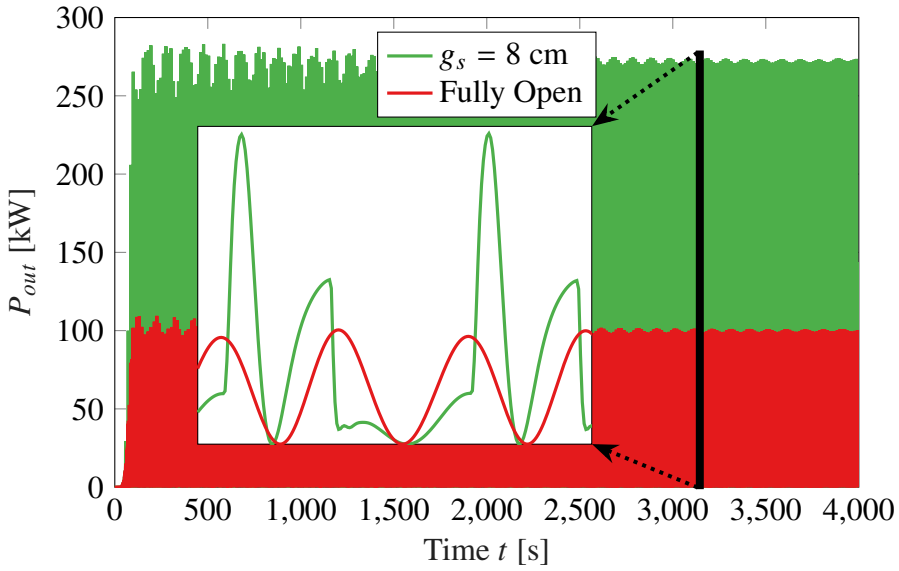

Figure 3.2: RM3 Power Output Responses for a Fully Open RM3 and when $g_s = 8$ cm; $H_s = 2$ m, $T_e = 13.5$ s

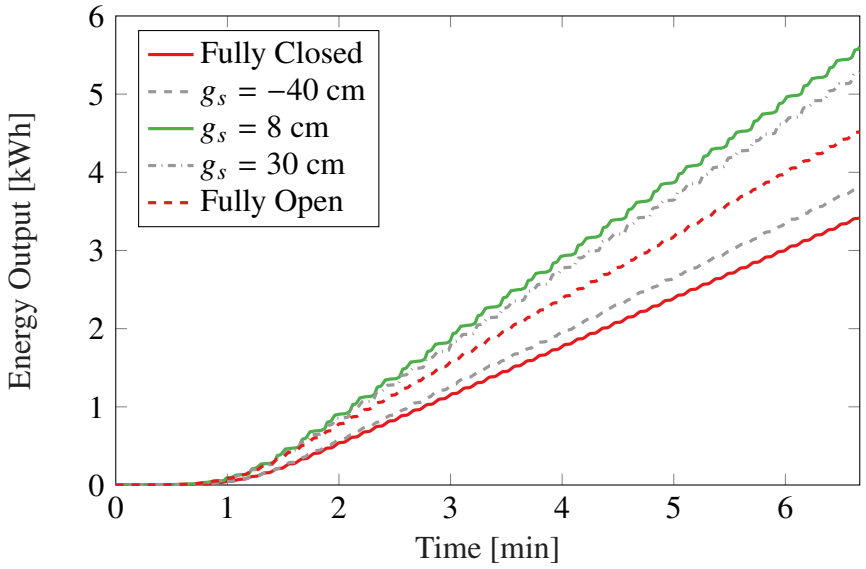

Figure 3.3: RM3 Energy Output for various stopper heights at $H_s = 2$ m, $T_e = 13.5$ s

fully closed (FC) region has a consistent $\bar{P}_{out}$ because the float and stopper never disengage, so that the effective damping of the RM3 is simply $c_e = c_{PTO} + c_s$. The intermittent contact (IC) region has an increase in $\bar{P}_{out}$ as g_s approaches 8 cm from the right because the float takes better advantage of the stopper. As g_s approaches FC from $g_s = 8$ cm, however, $\bar{P}_{out}$ decreases because the stopper suppresses the motion needed for mechanical energy. Note that in the FC region, $c_e = c_{PTO} + c_s$ and that in the FO region, $c_e = c_{PTO}$. Due to the continuity observed in Figure 3.4, it is speculated that c_e could be expressed as a piecewise function such that

$$c_e(g_s) = \begin{cases} c_s + c_{PTO} & g_s \in \text{FC} \\ c_{IC}(g_s) & g_s \in \text{IC} \\ c_{PTO} & g_s \in \text{FO}. \end{cases} \tag{3.1}$$

The nature of $c_{IC}(g_s)$ is not investigated here but left for future work.

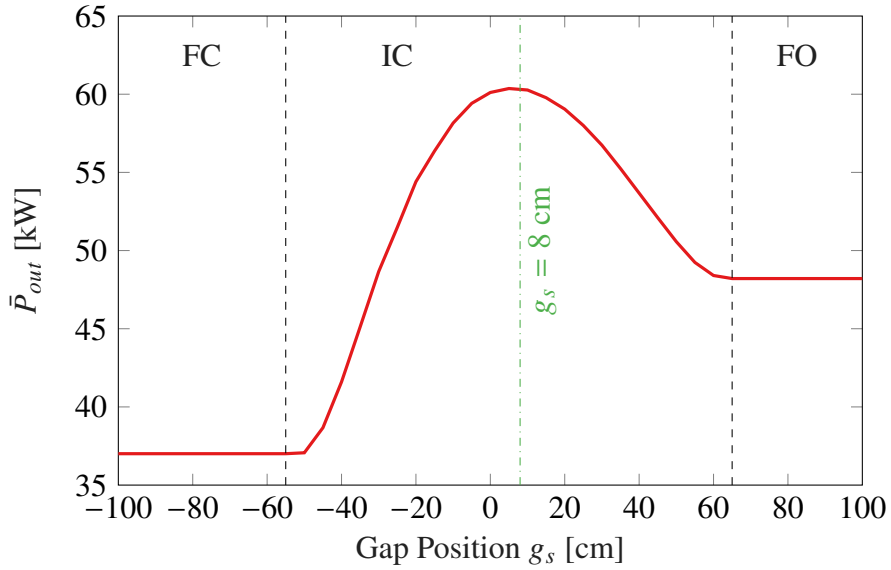

Figure 3.4: The effect of g_s on Average Power Output $\bar{P}_{out}$, $c_s = 5$ MNs/m, $k_s = 0$ N/m, $H_s = 2$ m, $T_e = 13.5$ s

Although decreasing the stopper gap below the recommended map gap decreases the power output, it also decreases the relative motion between the RM3's float and spar, shown in Figure 3.5, where the fully closed state exhibits motion control compared to the fully open or intermittent contact state. While WEC-Sim does not have the capacity to model high, or otherwise steep waves (as it is designed to handle waves within linear wave theory), it is suspected that this could be used to protect WECs in extreme sea states. Because the WEC can still generate power in the fully closed state, this would mean that WECs could still generate power in sea states that would otherwise cause too much relative motion between the two bodies for safe power generation.

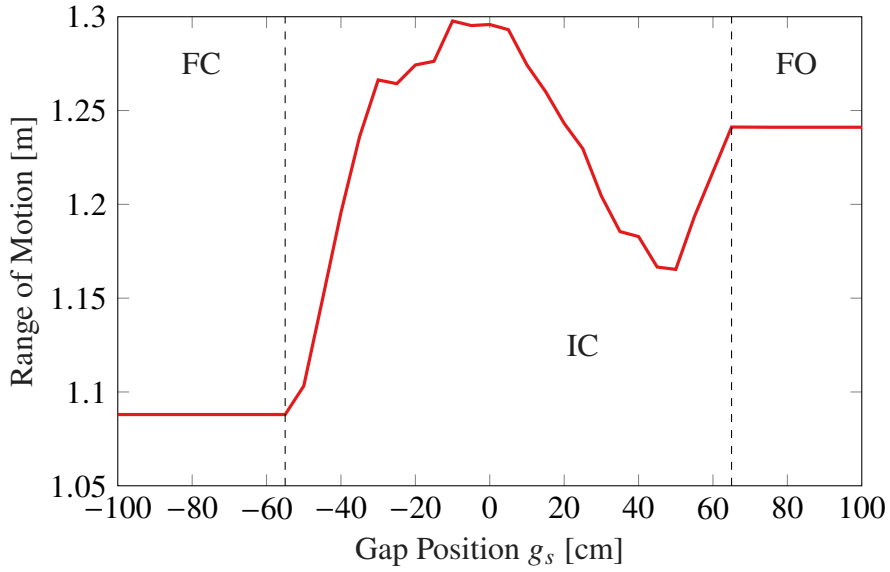

Figure 3.5: The Effect of g_s on the Steady-State Range of RM3 Relative Motion, c_s = 5 MNs/m, k_s = 0 N/m, H_s = 2 m, T_e = 13.5 s

3.2 Noisy Waves

To test the behavior of the controller in a more realistic environment, the open RM3 model was first tested with a wave condition of $H = 2$ m and $T = 13.5$ s for 4000 seconds, producing an average power output of 47.4 kW. Then two more cases were simulated to understand the behavior of the stopper-controlled RM3. The first used the same wave condition as the open model used, while the second added Gaussian noise with a magnitude of $0.1H_s$. A portion of this wave is shown in Figure 3.6, while the steady state response is shown in Figure 3.7.

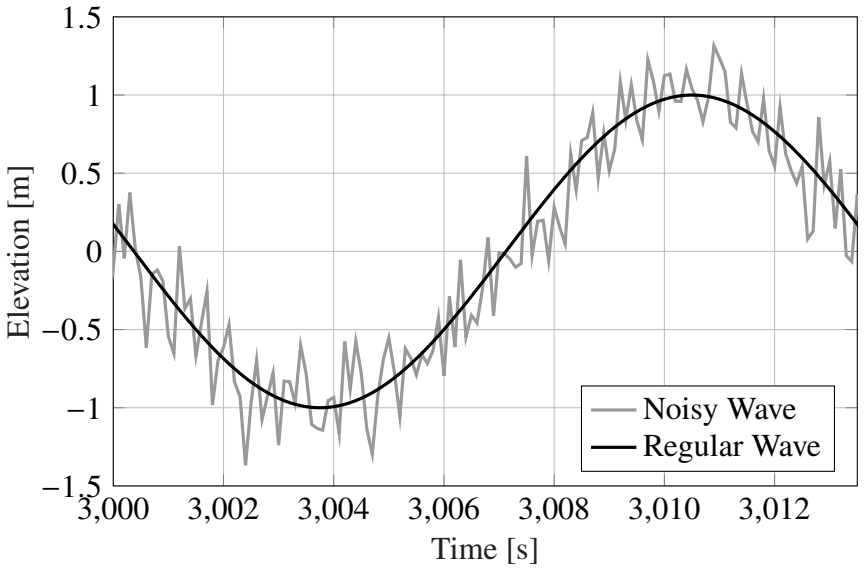

Figure 3.6: Close-Up View of Regular and Noisy Wave, $H_s = 2$ m, $T_e = 13.5$ s

With the regular wave, the stopper-controlled RM3 produced an average PTO power output of 58.9 kW, which has a 24.26% increase comparing to the open RM3 model power output. With the noisy wave, the average power output was also 58.9 kW, meaning that

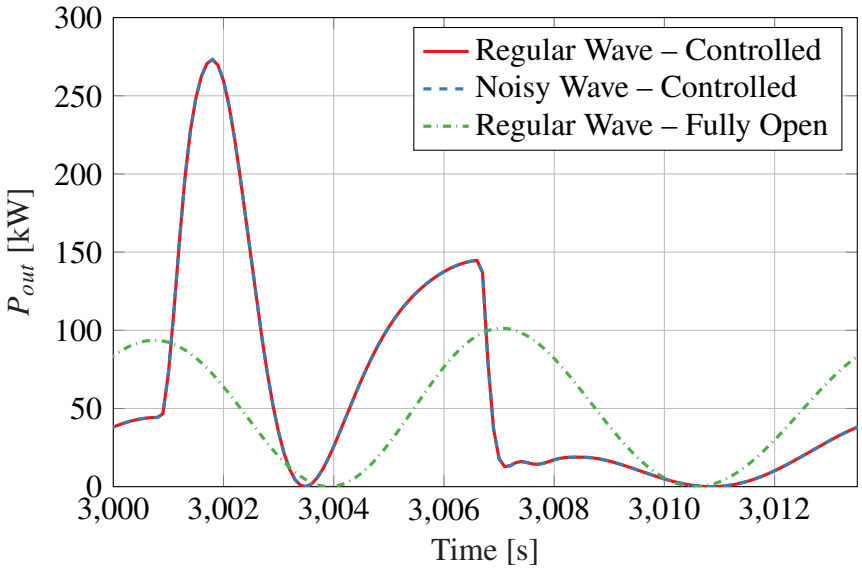

Figure 3.7: Close-Up view of Regular and Noisy Wave Response, $H_s = 2$ m, $T_e = 13.5$ s

the noise is negligible for the system response. This can be understood when considering Figure 2.5, as the selected stopper gap is constant in that region of sea states. This means that, even as the controller receives noisy data, the low-pass filter can easily filter it out, meaning the gap remains constant. Because the noise is small (only 10% of the wave height), the response is similar to when the stopper-controlled RM3 was tested against the regular wave of $H_s = 2$ m, $T_e = 13.5$ s.

The instantaneous power output P_{out} response of the fully open RM3 is relatively simple, following a periodic trend while oscillating in the water. To understand how the stopper-controlled RM3's P_{out} evolves through time, consider Figure 3.7. At $t \approx 3001$ s, the float engages the stopper at a high velocity. The stopper catches the float, exerting a large force into the float (and consequently, PTO) causing a large spike in power generation. At $t \approx 3003$ s, the float changes direction and continues to generate power with the influence

of the stopper force. At $t \approx 3007$ s, the stopper disengages, leading to a large loss in power generation. The stopper's velocity is low, resulting in a low power generation until the next period, when the float and stopper engage again. This contacting behavior, where most of the power generation occurs when $\Delta x_{rel} > g_s$, is shown in Figure 3.1.

Although the noise is negligible in this case, this is not generally true. While the low-pass filter is helpful in attenuating the effects of noise, it struggles to minimize the impact that noise in period measurements causes because the optimal gap size is very sensitive to period. This suggests the need for a more sophisticated filter design to better handle noise, especially in regions where the controller is highly sensitive to the sea period.

3.3 Quasistatic Waves

As an additional test to the stopper concept, the controlled-stopper RM3 model was subjected to various chirp waves to see how it would perform under quasi-static conditions. An example of a chirp wave is shown in Figure 3.8. Note that the quick change in height at the beginning results from the ramp function mentioned earlier. Data collected prior to the ramp time were neglected in data analysis.

Each chirp wave was designed to linearly transition over 4000 seconds from an instantaneous period of T_{e0} and height H_{s0} to T_{e1} and H_{s1}. The average power output for the open RM3 system $\bar{P}_{outO}$ and the stopper-controlled RM3 system $\bar{P}_{outS}$ were then compared. Table 3.1 show the results of the experiments containing the chirp waves. Interestingly, the waves whose periods decreased actually had a *decrease* in average power output compared to the open case. This is understandable, as the controller was designed with steady-state conditions in mind, and is not guaranteed to capture the dynamics of the system. This, of course, suggests the need for a more sophisticated controller architecture to better handle

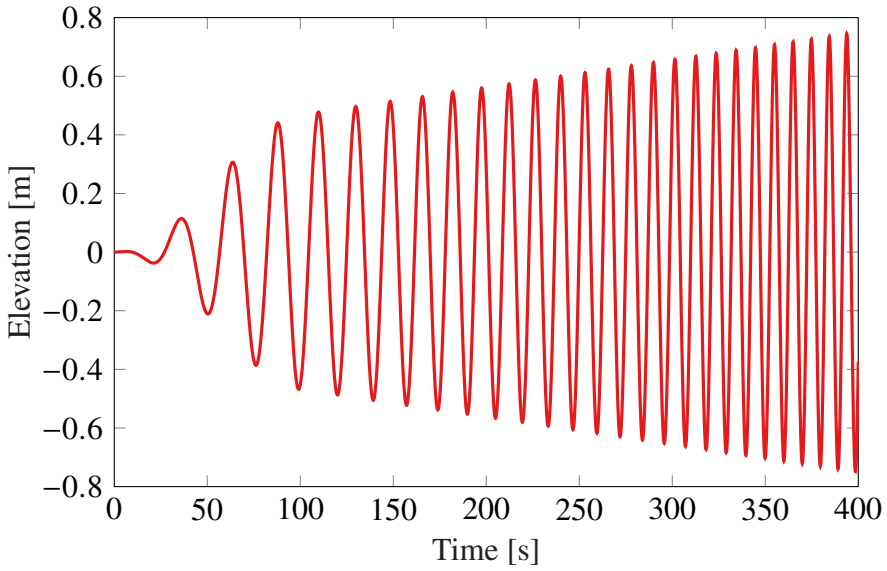

Figure 3.8: Example of a Linear Chirp Wave, $T_0 = 40$ s and $H_0 = 0.75$ m to $T_1 = 15$ s and $H_1 = 1.5$ m

the changing amplitude and height of the excitation and the fact that there is no stationary excitation.

H_{s0} [m]	H_{s1} [m]	T_{e0} [s]	T_{e1} [s]	$\bar{P}_{outO}$ [kW]	$\bar{P}_{outS}$ [kW]
0.75	0.75	11	14	8.14	7.08
0.75	1.50	11	14	17.2	14.0
0.75	0.75	14	11	13.0	14.3
0.75	1.50	14	11	34.3	36.5

Table 3.1: Summary of Chirp Wave Experiments

Chapter 4: Conclusions and Future Work

Dynamically-controlled stoppers have the potential to improve the average power output of wave energy converters (WECs) by improving the WEC's effective range of operation. A simple, damping-only stopper has been implemented in WEC-Sim, and its effects on the steady-state behavior of the Reference Model 3 (RM3) model have been characterized. Dynamic simulations have been investigated, and challenges for further development of the dynamically-controlled stopper have been identified.

Although the case studied here exhibits interesting properties, a more realistic case involving stopper stiffness and mass with stopper damping is needed to better understand the model's behavior under more realistic circumstances. Implementing a stopper mass in WEC-Sim and developing a strong understanding of its impact on the system is essential for using the concept in practice. Characterization of the intermittent contact effective damping as a function of gap size would be useful for developing variable-damping dampers.

After the implementation and testing of a stopper with mass, stiffness and damping, an analytical model will be useful for developing the idea further. While the computational method can consistently improve the power output of regular sea states, it struggles to handle noise and quasi-static cases. An analytical model characterizing the complete stopper, gap and RM3 interaction will be essential to developing a robust understanding of the system,

helping designers more easily choose a stopper configuration to meet the joint probability distribution of the site they are designing for.

An analytical model could also serve as the basis for a more sophisticated control algorithm. Controllers based on an analytical model (instead of experimentation) will almost certainly choose better gap sizes for regular sea states than obtained during this initial study, and will likely produce significant improvements in the power output observed in the noisy and quasi-static sea states. Developing an analytical control model will likely decrease the time it takes a designer to develop a control policy. The current process, developing power matrices for each stopper gap and comparing them to optimize for a performance metric, is computationally inefficient.

Following the development of an analytical model and a controller based on it, an essential step would be to test this idea in computational fluid dynamics (CFD) simulations. WEC-Sim is designed to handle linear sea states, and as such, struggles to model steep waves and more complicated wave phenomena such as wave breaking and wave slamming. Using CFD will provide the ability to determine how controlled-gap stoppers can impact WEC survivability and power output in extreme sea states that cannot currently be modeled in WEC-Sim. Moreover, the ability to lower the relative motion in these harsh sea states is a critical need in WECs. The proposed stopper implementation has this capability in addition to the increased power output at calmer sea states.

Bibliography

[1] WEC-Sim (Wave Energy Converter SIMulator) — WEC-Sim documentation.

[2] Tunde Aderinto and Hua Li. Ocean Wave Energy Converters: Status and Challenges. *Energies*, 11(5):1250, May 2018.

[3] B. Arnob and Md S. Advances and challenges in ocean wave energy harvesting. *Sustainable Energy Technologies and Assessments*, 61:103599, 2024.

[4] W. Cummins. *'The Impulse Response Function and Ship Motions.'*, volume 47. Schiffstechnik, 1962.

[5] H. Feng, C. Liu, W. Wang, Z. Dai, Zhang H., H. Ma, Y. Yalikun, B. Zhang, C. Shang, Y. Lai, and Yang Y. Omni-directional harvesting of ocean wave energy using arch-shaped double-layered direct-current triboelectric nanogenerator. *Nano Energy*, 132:110365, 2024.

[6] Y. Guan and K. D'Souza. A broadband piezoelectric energy harvester with robust control using piecewise nonlinearity. *Journal of Computational and Nonlinear Dynamics*, 02 2025.

[7] C. Knight, S. Mcgarry, J. Hayward, P. Osman, and S. Behrens. A review of ocean energy converters, with an australian focus. *AIMS Journal*, 2, 08 2013.

[8] M. Lawson, Y. Yu, K. Ruehl, and C. Michelen. Improving and validating the wec-sim wave energy converter modeling code. 3rd Annual Marine Energy Technology Symposium (METS). METS, apr 2015.

[9] A. Mohanty, S. Parida, R. Kumar Behera, and T. Roy. Vibration energy harvesting: A review. *Journal of Advanced Dielectrics*, 09(04):1930001, August 2019.

[10] M.A. Mustapa, O.B. Yaakob, Yasser M. Ahmed, Chang-Kyu Rheem, K.K. Koh, and Faizul Amri Adnan. Wave energy device and breakwater integration: A review. *Renewable and Sustainable Energy Reviews*, 77:43–58, September 2017.

[11] S. Nabavi, A. Farshidianfar, and A. Afsharfard. Novel piezoelectric-based ocean wave energy harvesting from offshore buoys. *Applied Ocean Research*, 76:174–183, 2018.

[12] V. Neary, M. Previsic, R. Jepsen, M. Lawson, A. Yu, Y .and Copping, A. Fontaine, K. Hallett, and D. Murray. Methodology for Design and Economic Analysis of Marine Energy Conversion (MEC) Technologies. 2014.

[13] K. Prajwal, K. Manickavasagam, and R. Suresh. A review on vibration energy harvesting technologies: analysis and technologies. *The European Physical Journal Special Topics*, 231(8):1359–1371, July 2022.

[14] R. So, C. Michelen, B. Bosma, P.a Lenee-Bluhm, and T. Brekken. Statistical Analysis of a 1:7 Scale Field Test Wave Energy Converter Using WEC-Sim. *IEEE Transactions on Sustainable Energy*, 8(3):1118–1126, July 2017. Conference Name: IEEE Transactions on Sustainable Energy.

[15] R. So, A. Simmons, T. Brekken, K. Ruehl, and Michelén S. Development of ptosim: A power performance module for the open-source wave energy converter code wec-sim. page V009T09A032, 05 2015.

[16] J. Tao, M. Hann, D. Greaves, and H. Shi. Numerical study of a point absorber wave energy converter with different power take-off systems. *Ocean Engineering*, 242:110181, 2021.

[17] M. Tien and K. D'Souza. Method for controlling vibration by exploiting piecewise-linear nonlinearity in energy harvesters. *Proceedings of the Royal Society A: Mathematical, Physical and Engineering Sciences*, 476:20190491, 01 2020.

[18] N. Tom, K. Ruehl, and F. Ferri. Numerical Model Development and Validation for the WECCOMP Control Competition: Preprint. June 2018.

[19] J. Veney and K. D'Souza. Frequency tunable electromagnetic vibration energy harvester using piecewise linear nonlinearity. *Proceedings of the Royal Society A: Mathematical, Physical and Engineering Sciences*, 479(2277):20230207, September 2023.

[20] N. Viet, X. Xie, K. Liew, N. Banthia, and Q. Wang. Energy harvesting from ocean waves by a floating energy harvester. *Energy*, 112:1219–1226, 2016.

[21] H. Yu, M. Lawson, K. Ruehl, and C. Michelen. DEVELOPMENT AND DEMONSTRATION OF THE WEC--SIM WAVE. 2014.

[22] F. Zeng, T. Wang, and J. Li. Origami-inspired dual-mode wave energy harvesting for ocean buoys. *Energy*, 320:135131, 2025.

Appendix A: Tuning the Rule-Based Controller

A.1 Introduction

This appendix discusses the programming done to develop the rule based controller mentioned in Section 2.3. It first details WEC-Sim's ability to run batches of simulations in parallel. It then details the development of a rudimentary data type to take advantage of this capability. Next, the CaseMatrix class is introduced to discuss the organization of the results. Then, the definition of performance metrics, and their implementation within the CaseMatrix class are discussed. Finally, the controller development is summarized, including how these components were used to develop it.

A.1.1 WEC-Sim's Parallel Capabilities

An essential component of WEC-Sim's architecture is its ability to run batches of simulations in parallel via MATLAB's Parallel Computing Toolbox. WEC-Sim users can run these batches in three main ways, but the most robust way is by calling a .mat file, specifically detailing the parameters for each simulation in the batch, from wecSimInputFile.m, the main script describing the simulation. Though these .mat files (called "mcr" files) can contain any data, they need to have two components:

- **mcr.header** – A $[1,\ n]$ cell array, with each cell containing the names of the parameters to be varied in the batch. These can be any parameter in wecSimInputFile.m, including standard WEC-Sim parameters (e.g., waves.period), or user-defined parameters.

- **mcr.cases** – An $[m,\ n]$ matrix containing the values of the parameters to be varied in the batch. Each row corresponds to a different simulation, and each column corresponds to a different parameter. The number of columns must be equal to the number of cells in mcr.header.

This method of running parallel simulations in WEC-Sim allows users to systematically run comparative simulations.

A.2 matMaker – Developing WEC-Sim Job Files

While WEC-Sim has a robust method for running batches of simulations in parallel, it does not provide a method for defining mcr files beyond simple cases involving WEC-Sim's built-in parameters. To specify mcr files complex enough for this thesis, a simple tool called "matMaker" was developed.

To use matMaker, the user specifies the parameters to be varied, along with their respective values. matMaker then develops a row in mcr.cases for each unique combination of parameters, and another cell array containing names corresponding to each variable and which is written to mcr.header. It also includes useful metadata in the .mcr file, including the number of unique values for each independent variable changed in the batch of simulations.

For example, if a user specifies 3 wave heights, 20 wave periods, 3 PTO damping values, and 2 PTO stiffness values, matMaker will generate a matrix with $3 \cdot 20 \cdot 3 \cdot 2 = 360$ rows and assign it to mcr.cases. A mcr.header cell array will be generated with 4 cells, with

each one containing the name of the variable associated with the corresponding column in mcr.cases.

Using matMaker enables users to run a batch of simulations with both built-in and custom parameters (such as the stopper stiffness, damping and gap), providing much more flexibility than WEC-Sim's built-in methods.

A.3 The CaseMatrix Class – Analyzing Parallelized WEC-Sim Jobs

WEC-Sim's parallel capabilities provide users with the ability to run batches of simulations, and matMaker gives users a simple and flexible way to make use of those capabilities. However, WEC-Sim does not provide a method to *analyze* the results it develops. To analyze the results developed by WEC-Sim, the "CaseMatrix" class was developed to organize them.

Suppose the user is interested in understanding how changing n different parameters affects the response of a WEC, with the i^{th} parameter considering p_i unique values. Because the matMaker function develops a simulation for each unique combination of values, the total batch of jobs can be represented as an n-dimensional matrix C_n (called a "CaseMatrix"), where each axis of C_n represents a parameter that varies within a batch of simulations. The length of the i^{th} axis of C_n is p_i, and the total number of cases m can be expressed by $m = \prod_{i=1}^{n} p_i$. Each cell of the matrix C_n contains a unique combination of values for each parameter, and the total number of cells in the matrix is equal to the total number of cases m. Because C_n is an n-dimensional matrix, it allows the user complete control over the analysis of the results, provided they understand matrix indexing in MATLAB.

Without loss of generality, a three-dimensional CaseMatrix (i.e. C_3), is shown in Figure A.1 as an example. There are three parameters being varied: The wave environment's

period, the wave environment's height, and the RM3's stopper gap (discussed extensively in Section 2.2). Each of these variables have three unique values, so there are 27 unique WEC responses in C_3. If, for example, a user wanted to understand how a WEC responds as the stopper gap varies, they would simply need to slice into different submatrices along the stopper gap dimension. Or, if the user wants to develop a frequency response for the WEC at a given height and stopper gap, they can investigate a $1 \times 1 \times 3$ submatrix along the wave period axis.

The CaseMatrix class defined in this work allows users to organize the results of parallel batches in n-dimensional matrices, allowing the user to analyze any arbitrary subset of the data they choose.

A.4 Defining Performance Metrics

With the data organized and easily accessible, performance metrics need to be defined to assess whether a given WEC response is *good*. While other performance metrics can be defined, the two performance metrics used in this thesis are:

- **Power Output** – The instantaneous mechanical power output of the WEC's power take off (PTO) system. This is essentially calculated by WEC-Sim, and is given by $P_{PTO} = v_{PTO} \cdot F_{PTO}$.

- **RM3 Relative Motion** – The relative motion between the RM3's float and spar. The calculation of the relative motion is described in Section 2.2. The relative motion is a good metric to represent the *survivability* of the WEC. Many two-body WECs are designed to have a limited range of motion between the two bodies, and exceeding that can damage them.

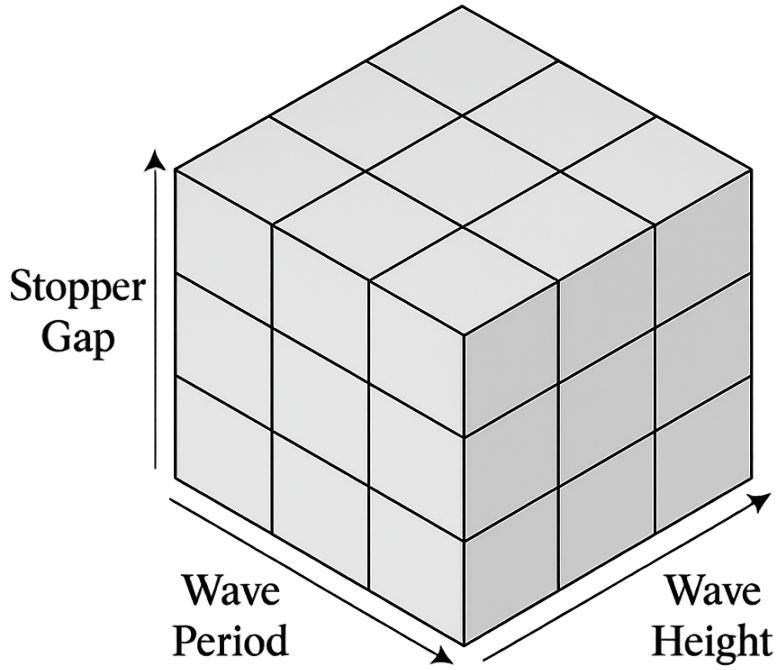

Figure A.1: An Example CaseMatrix. In this case, the CaseMatrix represents a batch of simulations with three varying parameters: the wave environment's period, the wave environment's height, and the RM3's stopper gap.

When considering a subset of cases, these performance metrics are calculated, and then manipulated to develop a single value indicative of the WEC's performance for a whole response. To develop power matrices, for example, the power output for the whole simulation can be called from the relevant elements of C_n. Then, all the time prior to the ramp time can be removed (to mitigate the effects of transients), and an estimate for the average power output can be calculated. This is shown in Figure A.2. Similarly, the range

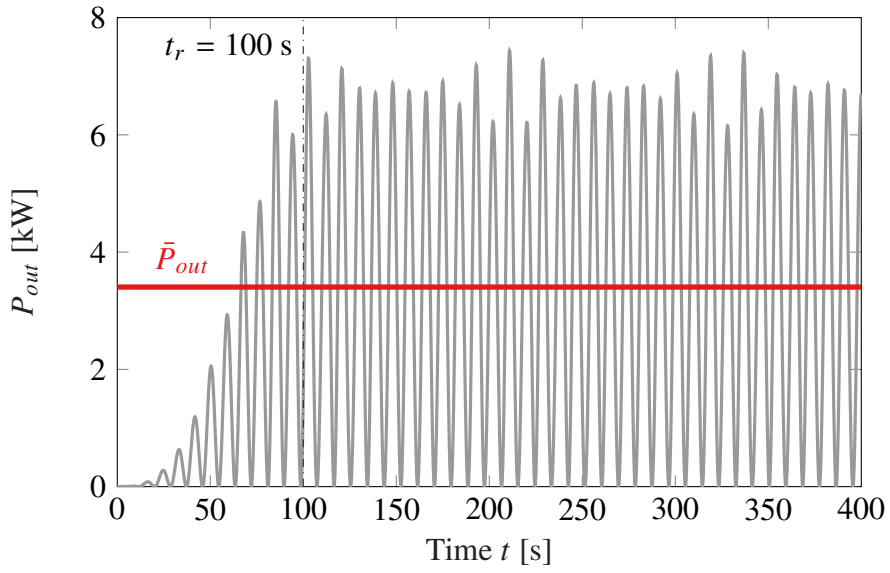

Figure A.2: Visual Explanation of the Average Power Output. Note that H_s = 1 m and T_e = 18 s.

of motion for a given case can be calculated by calling the relative motion for each time step of the response, neglecting data prior to the ramp time, and calculating the range of the remaining data.

A.5 Controller Development

To develop the controller described in Section 2.3, the steps taken are summarized as follows:

1. matMaker was used to develop a batch of simulations similar to the one shown in Figure A.1, though there were more values for each parameter to get a higher resolution of the WEC's response.

2. The resulting mcr file was run in WEC-Sim on a simple, uncontrolled-stopper RM3 model to assess how the stopper influenced the dynamic response of the system.

3. The CaseMatrix class was used to organize the results of the simulation into a 3D matrix whose dimensions corresponded to the varying parameters.

4. Using the power output performance metric and the processing described in Section A.4, the average power output was calculated for each case in the batch of simulations, resulting in a 3D matrix of average power outputs.

5. Using MATLAB's max function, the maximum average power along the stopper gap axis was calculated, and the corresponding stopper gap was recorded.

6. The stopper gaps corresponding to the maximum average power output were programmed into the controller.